

F. THE PHOBOS EXPERIMENT AT RHIC

The Phobos experiment has made significant progress over the past year. During the 2004 RHIC running Phobos collected a substantial data set for Au + Au collisions at energies of both $\sqrt{s_{NN}} = 200$ GeV and 62.4 GeV. The latter energy was chosen to be able to compare with pp collisions from CERN. A new large data set was also collected for $\sqrt{s_{NN}} = 200$ pp collisions. An upgrade of the Phobos data acquisition system allowed for substantially increased data rates, taking advantage of large improvements in the RHIC luminosity.

f.1. The Phobos Experiment at RHIC (B. B. Back for the Phobos Collaboration*)

The present status of Phobos physics results has been summarized in a recent white paper,¹ which will be published in Nucl. Phys. A along with similar status papers from the other three RHIC experiments. Based on these white papers there is a general consensus among the experiments that the following discoveries has been made at RHIC:

- 1) A new form of matter, which cannot be described in terms of hadronic degrees of freedom has been produced in head-on Au + Au collisions.
- 2) This matter has an energy density, which substantially exceeds the theoretical threshold for entering the quark-gluon plasma phase.
- 3) The observation of collective flow patterns in the particle emission point to a strongly interacting, essentially ideal fluid description of this matter.
- 4) The disappearance of back-to-back high- p_T particles expected for hard parton scattering indicates that this matter is highly opaque because of a high density of unscreened color charges.

At this point, the RHIC research has thus achieved a rough characterization of this new form of matter. Some of the results are contrary to the naïve expectation that a weakly interacting quark-gluon plasma may be formed. The strongly interacting nature and the opaqueness were surprises. These results are expected to substantially advance our

understanding of the quantum chromodynamics theory of the strong interaction, especially as it relates to the temperature regimes probed in these reactions.

In the following, several new results obtained by the Phobos collaboration will be discussed.

Centrality Dependence of D + Au Multiplicities

The centrality dependence of charged particle emission in 200 GeV d + Au collisions has been studied. Figure I-42 shows the pseudorapidity distributions, $dN/d\eta$, for five centrality bins with the pseudorapidity, η , being measured relative to the deuteron beam direction.² We observe that the distribution for the most central collisions (0-20%) is quite asymmetric relative to $\eta = 0$. This effect is believed to reflect the fact that for these collisions about 13.5 nucleons from the Au nucleus participate in the reaction with the two nucleons in the deuteron. Momentum conservation therefore demands that more particles be emitted in the direction of the incoming Au nucleus. We observe also that this asymmetry subsides for the more peripheral collisions such that an almost symmetric distribution is observed for the 80-100% bin, which involves about 1.6 Au nucleons and 1.1 deuteron nucleons, on average. Guided by the “extended longitudinal scaling” observed in hadronic collisions we are able to obtain the total number of charged particles via an extrapolation into the unmeasured regions.² The consequences of a further analysis of these results are discussed in the following section.

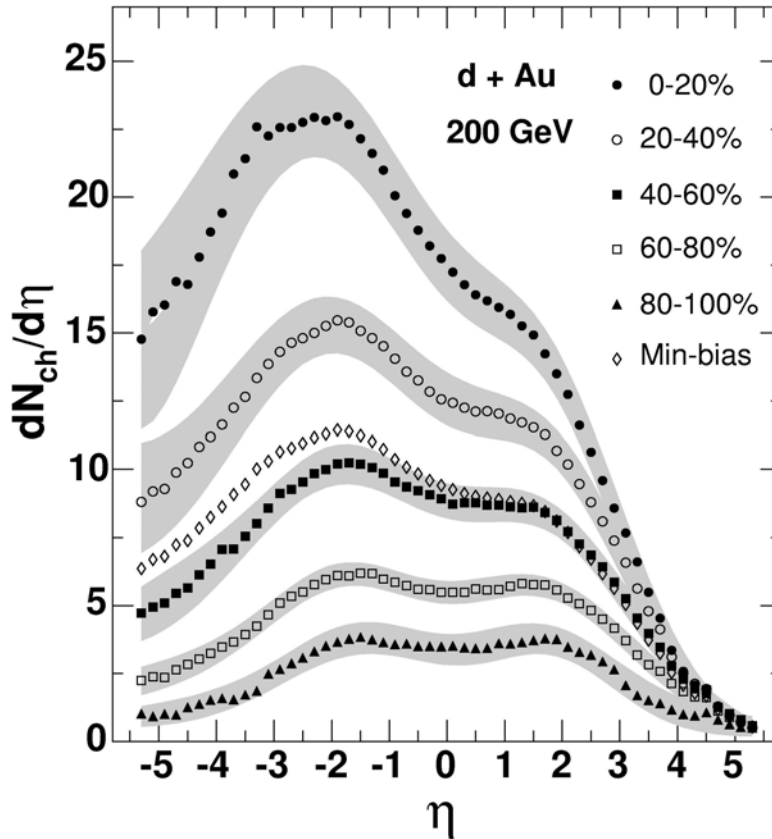


Fig. I-42. Distribution of pseudorapidity densities of charged particles emitted in $d + Au$ collisions at $\sqrt{s_{NN}} = 200$ GeV for five centrality bins.² The positive pseudorapidity direction is that of the deuteron. The centrality is designated by the fraction of the total inelastic cross section, with smaller numbers being more central. Grey bands indicate the systematic uncertainties (90% C.L.).

Scaling in Charged Particle Production

Because the Phobos multiplicity detector covers an angular range from $\theta = 0.5^\circ$ to 179.5° it is possible, with a very small extrapolation, to obtain the total number of charged particles emitted in a collision. By studying $Au + Au$ collisions as a function of centrality, we have found that the total number of charged particles, N_{ch} , scales rather rigorously with the number of participant pairs, $N_{part}/2$, in the collision, such that the ratio $N_{ch}/N_{part}/2$ is essentially constant as a function of centrality as illustrated in Fig. I-43 (solid points).³ This scaling feature also applies to the simpler $d + Au$ collisions (open points), but we note that the charged particle production rate in this case is substantially lower (by about 40%),

which is at the level observed in proton-proton collisions at the same energy⁴ (solid square). The enhanced charged particle production in $Au + Au$ collisions does not appear to be simply a consequence of the number of participants in the collisions because there is no indication of an increased multiplicity even for the most central $d + Au$ collisions. We also note that the multiplicity for e^+e^- collisions⁵ is consistent with the heavy-ion data. A possible explanation for this disparity between nucleon-induced and heavy-ion or lepton induced collisions is the fact that leading particles in nucleon-induced collisions carry away about half of the energy, which is then not available for particle production.⁶ It is surprising, however, that this mechanism is still effective in $d + Au$ collisions, which involve a substantial number of subsequent collisions.

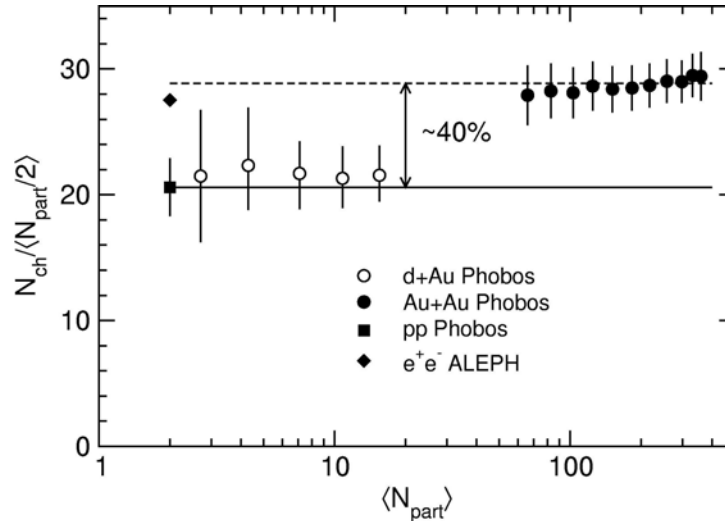


Fig. I-43. $N_{ch}/N_{part}/2$ for Au + Au⁶ (solid points), d + Au¹ (open circles) are shown as a function of N_{part} and compared to values for pp⁴ (solid square) and e⁺e⁻ (solid diamonds) collisions. The horizontal dashed line represents the average value for Au + Au collisions, which is ~40% higher than the pp level (solid line).

Multiplicity Scaling in Au + Au Collisions at 19.6 and 200 GeV

At all Au + Au collision energies, we have found that the pseudorapidity density, $dN/d\eta$ at midrapidity, $\eta = 0$, increases with centrality (N_{part}) in a smooth fashion. This increase was attributed to hard collisions (between partons) since such collisions are expected to scale roughly with $N_{part}^{4/3}$ and therefore assume increased importance in central collisions. Furthermore, it was assumed that the hard processes would prevail with increasing collision energy. Recently we have found, however, that the increase

in multiplicity with centrality is the same in Au + Au collisions at 19.6 and 200 GeV as illustrated in Fig. I-44, see Ref. 7. Here the ratio, $dN/d\eta(200)/dN/d\eta(19.6)$ is seen to be flat as a function of centrality indicating that the fraction of hard collisions is constant with collision energy. In fact, since the centrality dependence of $dN/d\eta$ is independent of collision energy there is a straight factorization of $dN/d\eta$, which may be expressed as: $dN/d\eta(s, N_{part}) = f(s) g(N_{part})$.

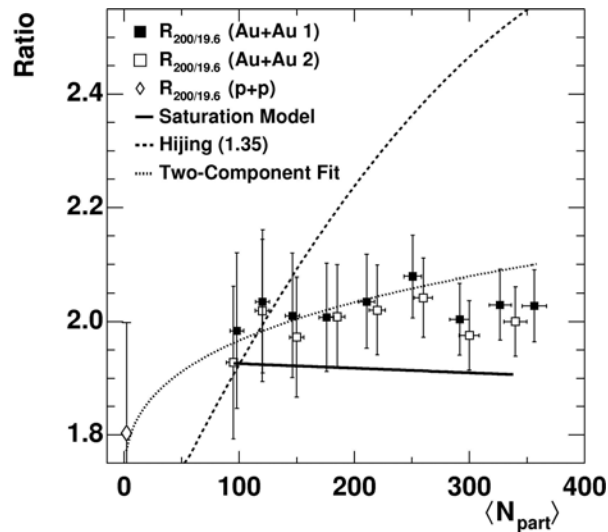


Fig. I-44. The ratio, $R_{200/19.6}$ of the multiplicity density per participant pair at 200 and 19.6 GeV versus $\langle N_{part} \rangle$ binned by fraction of cross section (closed circles) and by matching $\langle N_{part} \rangle$ (open squares).⁷ The ratio of inelastic p + p collision data is given at $N_{part} = 2$ (open diamond). Curves give various calculations. The vertical error bars are combined statistical and systematic 1- σ uncertainties.

Elliptic Flow

One of the important discoveries at RHIC is that of elliptic flow, *i.e.* the preferential emission of particles at azimuthal angles corresponding to the reaction plane between the two interacting ions. The elliptic flow is measured in terms of the second Fourier coefficient of the particle azimuthal angular distribution $v_2 = \langle \cos[2(\psi - \psi_{\text{reac}})] \rangle$, where $\psi - \psi_{\text{reac}}$ is the azimuthal angle of the emitted particle relative to that of the reaction plane. The average is extended over all particles emitted within a certain pseudorapidity interval in each event. Figure I-45 shows the elliptic flow signal as a function of event centrality, given in terms of N_{part} , (left panel) and

particle transverse momentum (right panel).⁸ The data are in remarkable agreement with the predictions of a hydrodynamic model (solid lines),⁹ which indicates that the matter formed in these collisions behave much like an ideal, non-viscous liquid. This observation, which is in accord with those from the other three RHIC experiments, is contrary to the original naïve expectation that matter in the Quark Gluon Plasma phase behave as a weakly interacting gas. The observation of a strong collective flow signal in heavy-ion collisions at RHIC energies is thus a first, but important, step in the characterization of this new phase of matter.

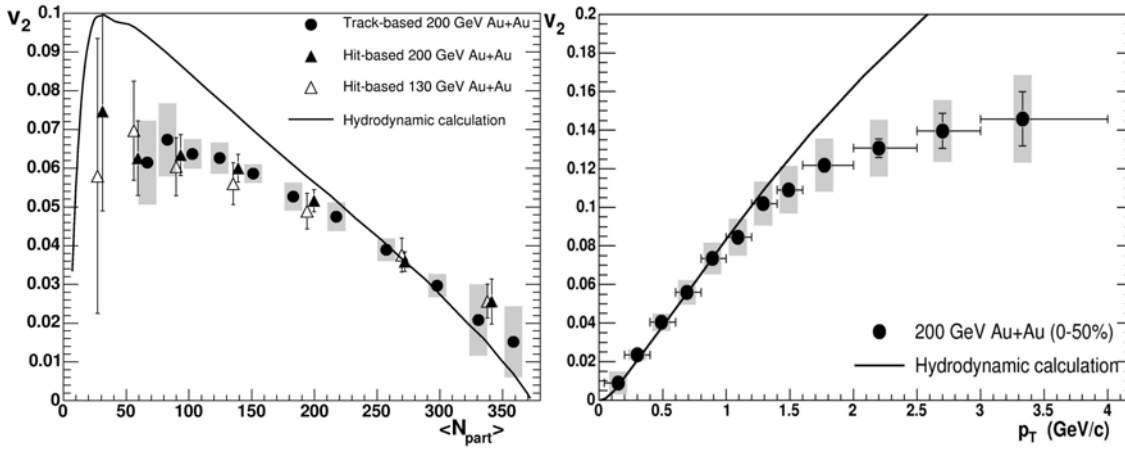


Fig. I-45. Left panel: Elliptic flow ($v_2(|\eta| < 1)$) as a function of $\langle N_{\text{part}} \rangle$ determined by the track-based method (closed circles) and hit-based method (closed triangles) for Au + Au collisions at 200 GeV.⁸ The open triangles are the $v_2(|\eta| < 1)$ as a function of $\langle N_{\text{part}} \rangle$ results from Au + Au collisions at 130 GeV. The line shows a calculation from hydrodynamics⁹ at $\sqrt{s_{\text{NN}}} = 200$ GeV. The grey boxes show systematic uncertainties for the 200 GeV results from the track-based method. Right panel: Elliptic flow as a function of transverse momentum, $v_2(p_T)$, for charged hadrons with $0 < \eta < 1.5$ for the most central 50% of the 200 GeV Au + Au collision cross section.⁷ The grey boxes represent the systematic error. The data points are located at the average p_T position with a p_T bin whose size is given by the horizontal error bars. The curve shows a calculation from hydrodynamics.⁹

The ability of Phobos to measure charged particles over a very wide angular range allows us to also perform unique, complete measurements of the elliptical flow signal. Such results are shown for three centrality bins in Fig. I-46 for Au + Au collisions at 200 GeV. We observe an interesting strong peaking of the v_2 signal at mid-rapidity followed by an immediate fall-off at both positive

and negative values of η . Although the hydro-dynamical models have been quite successful in describing the v_2 signal at mid-rapidity, such models have had difficulties explaining the rapid falloff seen experimentally. Recently, however, it appears that the Buda-Lund version of the hydro-dynamic model is able to reproduce the η -dependence seen in the Phobos results by including the effects of a directed flow (v_1 component).¹⁰

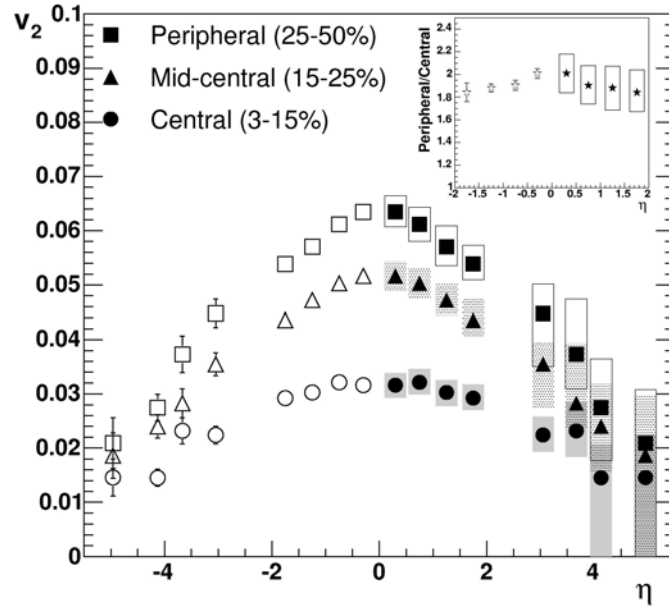


Fig. I-46. Elliptic flow as a function of pseudorapidity, $v_2(\eta)$, for charged hadrons from 200 GeV Au + Au collisions for three different centrality classes.⁸ The data for $\eta > 0$ are determined by reflecting the hit-based results about mid-rapidity and combining them with the track-based results and shown with the systematic errors only. The same data are reflected around $\eta = 0$ and shown as open symbols with statistical errors only. The inset shows the ratio of the peripheral to central combined results where the two methods overlap, with only statistical errors shown for $\eta < 0$ and only systematic errors for $\eta > 0$.

In Fig. I-47 we show the elliptic flow signal, v_2 , for 0-40% central collisions for all four energies studies so far. The data are plotted vs. the parameter $\eta' = |\eta| - y_{\text{beam}}$, where y_{beam} is the beam rapidity. We have previously shown¹¹ that the charged-particle production, $dN/d\eta$ obeys limiting fragmentation scaling i.e. $dN/d\eta$ is independent of collisions energy

in the region near η' . It is now interesting to observe that a similar scaling behavior applies to the elliptical flow signal as demonstrated in Fig. I-47. Because of the universality of this scaling behavior the term ‘extended longitudinal scaling’ has been attached to this feature. No satisfactory theoretical explanation for this scaling has been put forth.

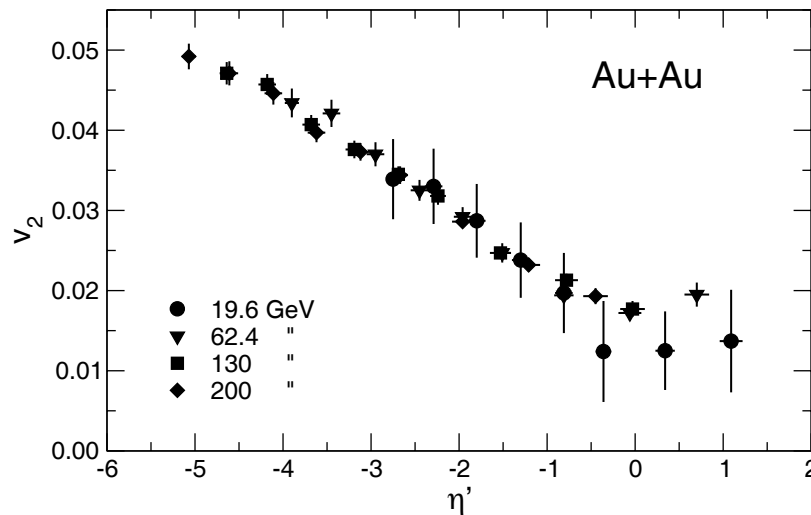


Fig. I-47. Elliptic flow, averaged over centrality (0-40%), as a function of $\eta' = |\eta| - y_{\text{beam}}$ for four collision energies for the Au + Au system.¹² The error bars represent 1σ statistical errors only.

Hanbury-Brown/Twiss Analysis of Two-Particle Correlations

The method of analysis of two-photon correlations from astronomical objects to estimate their radial extent is well established.¹³ This method can also be applied to estimate the spatial extent of the fireball created in heavy-ion collisions at ultra-relativistic energies. In Phobos we have performed such an analysis based on pairs of pions, which are detected and momentum analyzed in the Phobos spectrometer. Experimentally the correlation function is defined as

$$C(\vec{q}) = \frac{P(\vec{p}_1, \vec{p}_2)}{P(\vec{p}_1)P(\vec{p}_2)}$$

where \vec{p}_1 and \vec{p}_2 are the particle four-momenta with relative four-momentum $\vec{q} = \vec{p}_1 - \vec{p}_2$ and $P(\vec{p}_1)$ and $P(\vec{p}_2)$ are single-particle probabilities. The numerator is determined directly from the data, while the denominator is constructed using a standard event-mixing technique. The experimentally determined correlation function $C(\vec{q})$ can be fit to the Bertsch-Pratt¹⁵ parameterization of a Gaussian source in three dimensions

$$C(\vec{q}) = 1 + \lambda e^{-(q_0^2 R_0^2 + q_s^2 R_s^2 + q_l^2 R_l^2 + 2q_0 q_l R_{0l}^2)},$$

where q_l is the component of \vec{q} along the beam direction, q_0 is the component along the pair transverse momentum $k_T = \frac{1}{2}(\vec{p}_{T1} + \vec{p}_{T2})$, and q_s is the component orthogonal to the other two. Results of such an analysis are shown in Fig. I-48 and compared with data from other experiments at RHIC energies, as well as studies at lower collision energies at the CERN SPS and the Brookhaven AGS facilities. First we observe that the results of the Phobos analysis agree well with those from other experiments. Of particular interest is the ratio between the “out” and “side” dimension of the source at freeze-out, R_o/R_s . This ratio is found to be near unity at both energies (left panel), whereas hydrodynamical models of the expansion of the fireball predicts values of the order $R_o/R_s \sim 1.5-2.0$.¹⁹ This discrepancy is observed by all RHIC experiments and has not yet been understood although a recent publication²⁰ suggests that a quantum-mechanical treatment of the opacity and refractive effects in the fireball may partly contribute to this effect.

*Brookhaven National Laboratory, Institute of Nuclear Physics, Krakow, Poland, Massachusetts Institute of Technology, National Central University, Taoyuan, Taiwan, University of Rochester, University of Illinois-Chicago, and University of Maryland.

¹B. B. Back *et al.*, Nucl. Phys. **A757**, 28 (2005).

²B. B. Back *et al.*, Phys. Rev. C **72**, 031901 (2005).

³B. B. Back *et al.*, Intl. J. Mod. Phys. A (2005).

⁴R. Nouicer *et al.*, J. Phys. G **30**, 51133 (2004).

⁵H. Stenzel *et al.*, Eur. Phys. J. C **35**, 457 (2004).

⁶P. Steinberg *et al.*, Nucl. Phys. **A715**, 490c (2003).

⁷B. B. Back *et al.*, Phys. Rev. C **70**, 021902R (2004).

⁸B. B. Back *et al.*, Phys. Rev. C **72**, 051901 (2005).

⁹P. Kolb *et al.*, Phys. Lett. **B500**, 232 (2001).

¹⁰M. Csanad, T. Csorgo, B. Lorstad, and A. Ster, J. Phys. G **30**, 1079 (2004).

¹¹B. B. Back *et al.*, Phys. Rev. Lett. **91**, 052303 (2003).

¹²B. B. Back *et al.*, Phys. Rev. Lett. **94**, 122303 (2005).

¹³R. Hanbury-Brown and R. Q. Twiss, Phil. Mag. Ser. 7, Vol. **45**, No. 366, 663 (1954); Nature **178**, 1046 (1956).

¹⁴B. B. Back *et al.*, accepted for publication in Phys. Rev. C; nucl-ex/0409001.

¹⁵S. Pratt, Phys. Rev. D **33**, 1314 (1986); G. Bertsch, Nucl. Phys. **A498**, 173 (1989).

¹⁶J. Adams *et al.*, Phys. Rev. Lett. **93**, 012301 (2004).

¹⁷S. S. Adler *et al.*, nucl-ex/0401003.

¹⁸C. Adler *et al.*, Phys. Rev. Lett. **87**, 082301 (2001); K. Adcox *et al.*, Phys. Rev. Lett. **88**, 192302 (2002);

L. Ahle *et al.*, Phys. Rev. C **66**, 054906 (2002); D. Adamova *et al.*, Nucl. Phys. **A714**, 124 (2003); M. A. Lisa *et al.*,

Phys. Rev. Lett. **84**, 2798 (2000); I. G. Bearden *et al.*, Phys. Rev. C **58**, 1656 (1998); S. Kniege *et al.*, nucl-

ex/0403034; M. M. Aggarwal *et al.*, Eur. Phys. J. C **16**, 445 (2000).

¹⁹U. W. Heinz and P. F. Kolb, hep-ph/0204061.

²⁰J. G. Cramer, G. A. Miller, J. M. S. Wu, and J. H. Yoon, Phys. Rev. Lett. **94**, 102302 (2005).

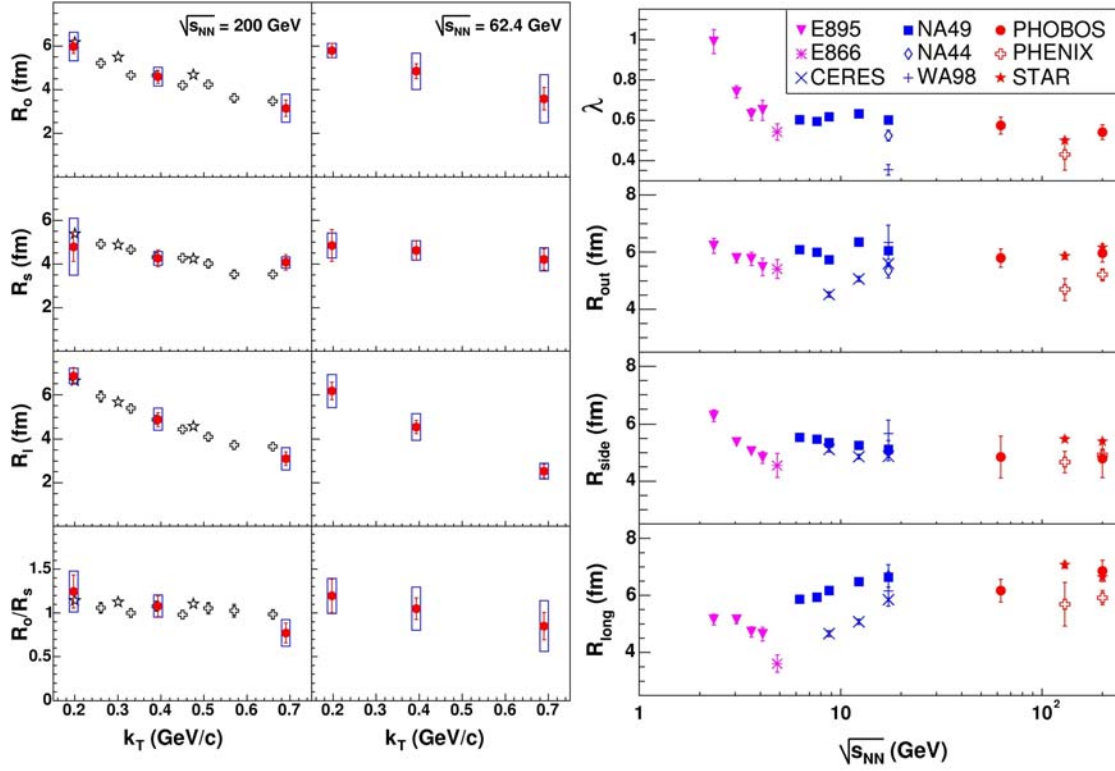


Fig. I-48. Left figure: Bertsch-Pratt parameters R_o , R_s , R_l and the ratio R_o/R_s for $\pi^+\pi^-$ pairs at 200 GeV (left panel) and 62.4 GeV (right panel) Au + Au collisions as a function of $\langle k_T \rangle$.¹⁴ For comparison, data from STAR¹⁶ (open stars) and PHENIX¹⁷ (open crosses) are presented at 200 GeV. Phobos systematic errors (90% C.L.) are shown as boxes; systematic errors from STAR and PHENIX are not shown. Right figure: Bertsch-Pratt parameters λ , R_{out} , R_{side} , R_{long} as a function of $\sqrt{s_{NN}}$ for $\pi^+\pi^-$ pairs. The presented data are near mid-rapidity and represent comparable k_T bins from each experiment.¹⁸ Phobos data are represented by solid circles. Systematic errors are not shown.

